COMBINED RADIATION-NATURAL CONVECTION IN THREE-DIMENSIONAL VERTICALS CAVITIES.

by

Lioua KOLSI*, Awatef ABIDI, Chemseddine MAATKI, Mohamed Naceur BORJINI, and Habib BEN AISSIA

Ecole Nationale d'Ingénieur de Monastir, Monastir, Tunisia.

In this article we studied the effect of radiative transfer and the aspect ratio on the 3D natural convection. Prandtl and Rayleigh numbers are respectively fixed at 13.6 and 10^5. Equations of natural convection are expressed according the vorticity-stream function formulation. This equations and radiative transfer equation are respectively descritized by volume control method and the FTnFVM. Obtained simulation show that the principal flow structure is considerably modified when the radiation-conduction parameter was varied. However, the peripheral spiraling motion is qualitatively insensitive to these parameters.

Keywords: natural convection, radiation, 3D vertical cavities, spiral flow.

1. Introduction

Natural convection problem in tall vertical cavity was the object of many experimental and numerical studies. The majority of studies in 3D geometries are realized for cubical cavities [1-18]. Tric et al. [10] find precise solutions of this problem using the Chebyshev pseudo-spectral algorithm. Pepper and Hollands [11] analyzed numerically the case of 3D natural convection of a filled air cavity. To simulate this case, recently Wakashima and Saitoh [12] used the high-order time–space method. Several other authors were interested in the analysis of the three-dimensional structures in the case of the air ([1] and [5]), of the molten metals ([14-18]) and of the great Prandtl numbers fluids ([3] and [4]). Studies, of Hiller et al. [3] and of Mallinson and Davis [1], show that the three-dimensional structure of the flow comprises one or two inner spiraling motions sustaining the transverse flow between the front or back walls and the center of the box and a large spiraling flow near the lateral walls. This transverse flow was also identified in the metals molten (Viskanta et al. [14]). The majority of the studies [19-23] relating to the combined radiation-natural convection in rectangular semi-transparent mediums are in the 2D case. Recently Colomer et al. [24] analyzed this problem in the 3D case while being interested particularly in the effect the optical thickness on the heat transfer and give a comparison between the two-dimensional results and those obtained in the median plane of a lengthened rectangular enclosure.

However these authors were not interested in the study of the effect of the radiation on the transverse spiraling flow, which we propose to undertake in this work.

In this work we propose to carry out a study of the effect of the radiation on 3D natural convection of the $LiNbO_3$ in vertically lengthened enclosures for, Ra = 10^5 and for various optical properties. $LiNbO_3$ single crystal is an excellent material for various optical applications; natural convection and radiation have a direct effect on its crystalline growth.

After the formulation of the problem and some validations, the first results relate to the principal flow and the heat transfer and the second relate to the spiraling transverse flow.

2. Formulation

Figure 1, presents the considered physical system which is composed of a square basic parallelepipedic enclosure, with aspect ratio Ar=H/W and with different uniform temperatures imposed on two opposite vertical walls, whereas all the other walls are adiabatic. One assumes that all these surfaces are gray and diffuse. This cavity is filled with a gray, emitting–absorbing and isotropically scattering fluid. The flow is supposed to be laminar and the Boussinesq approximations are used.

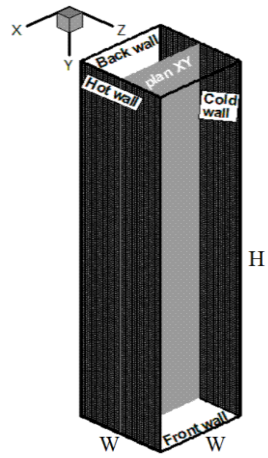

Figure 1. Model Presentation

The equations describing the combined radiation-natural convection are the equations of continuity, of momentum and of energy:

$$\nabla.\vec{V}'=0 \tag{1}$$

$$\frac{\partial \vec{V}'}{\partial t'}+(\vec{V}'.\nabla)\vec{V}'=-\frac{1}{\rho}\vec{\nabla}P'+\nu\Delta\vec{V}'+\beta_t(T'-T_0)\vec{g} \tag{2}$$

$$\frac{\partial T'}{\partial t'}+\vec{V}'.\nabla T'=\alpha\nabla^2 T'-\frac{1}{\rho c_p}\vec{\nabla}q'_r \tag{3}$$

As numerical method we had recourse to the vorticity-vector potential formalism $(\vec{\psi}-\vec{\omega})$ which allows, in a 3-D configuration, the elimination of the pressure, which is a delicate term to treat. To eliminate this term one applies the rotational to the equation of momentum. The vector potential and the vorticity are, respectively, defined by the two following relations:

$$\vec{\omega}'=\vec{\nabla}\times\vec{V}' \text{ and } \vec{V}'=\vec{\nabla}\times\vec{\psi}' \tag{4}$$

In the equations (1, 2 and 3), time t', velocity $\vec{V}'$, the stream function $\vec{\psi}'$, the vorticity $\vec{\omega}'$, are put respectively in their adimensional forms by W^2/α, α/W, α and W^2/α : and the adimensional temperature is defined by: $T=(T'-T_c')/(T_h'-T_c')$.

After application of the $(\vec{\psi}-\vec{\omega})$ formalism and adimensionalisation the system of equations controlling the phenomenon becomes:

$$-\vec{\omega}=\nabla^2\vec{\psi} \tag{5}$$

$$\frac{\partial\vec{\omega}}{\partial t}+(\vec{V}.\nabla)\vec{\omega}-(\vec{\omega}.\nabla)\vec{V}=\Delta\vec{\omega}+Ra.\Pr.\left[\frac{\partial T}{\partial z};0;-\frac{\partial T}{\partial x}\right] \quad (6)$$

$$\frac{\partial T}{\partial t}+\vec{V}.\nabla T=\nabla^2 T+\frac{Rc.\tau}{\Phi_t.\pi}(1-\omega_0).\left[\int_{4\pi} I.d\Omega-4.\pi.(1+\Phi_t T)^4\right] \quad (7)$$

With $\Pr=\nu/\alpha$, $Ra=\frac{g.\beta_t.W^3.(T_h^{'}-T_c^{'})}{\alpha.\nu}$, $Rc=i^2.W.T'^3_c.\sigma/\lambda$, $\tau=\kappa.W$ and $\Phi t=T_h^{'}/T_c^{'}-1$

The boundary conditions are given as:

- Temperature

$T=1$ at $x=1$, $T=0$ at $x=0$; $\frac{\partial T}{\partial n}=0$ on other walls (adiabatic).

- Vorticity

$\omega_x=0$, $\omega_y=-\frac{\partial V_z}{\partial x}$, $\omega_z=\frac{\partial V_y}{\partial x}$ at $x=0$ and 1 ; $\omega_x=\frac{\partial V_z}{\partial y}$, $\omega_y=0$, $\omega_z=-\frac{\partial V_x}{\partial y}$ at $y=0$ and 1 ; $\omega_x=-\frac{\partial V_y}{\partial z}$, $\omega_y=\frac{\partial V_x}{\partial z}$, $\omega_z=0$ at $z=0$ and 1

- Vector potential

$\frac{\partial\psi_x}{\partial x}=\psi_y=\psi_z=0$ at $x=0$ and 1; $\psi_x=\frac{\partial\psi_y}{\partial y}=\psi_z=0$ at $y=0$ and 1 ; $\psi_x=\psi_y=\frac{\partial\psi_z}{\partial z}=0$ at $z=0$ and 1

- velocity

$V_x=V_y=V_z=0$ on all walls

- Radiative flux

$-\frac{\partial T}{\partial y}+q_r Rc/\Phi=0$ at y=0 and y=1 ; $-\frac{\partial T}{\partial z}+q_r Rc/\Phi=0$ at z=0 and z=1

The radiative transfer equation, for a gray semi-transparent medium which isotropically absorbs, emits and diffuses the radiation**,** can be written:

$$\frac{\partial I(s,\vec{\Omega})}{\partial s}+\beta I(s,\vec{\Omega})=\beta R \quad (8)$$

with : $$R=(1-\omega_0)I^0(s)+\frac{\omega_0}{4\pi}\int_{4\pi} I(s,\vec{\Omega}')\,d\Omega' \quad (9)$$

The classical of finished volumes method divides the field studied into a finished number of controls volumes and the intensity direction in a finished number of solid angles. The control solid angle $\Delta\Omega^l$ is given by:

$$\Delta\Omega^l=\int_{\theta^{l-}}^{\theta^{l+}}\int_{\varphi^{l-}}^{\varphi^{l+}} \sin\theta\, d\theta\, d\varphi \quad (10)$$

l indicates a discrete direction and θ and φ are respectively polar and azimuth angles. Integration of equation (8) in a control volume Δv centered in P **(**fig. **2)** and in a control angle $\Delta\Omega^l$ gives:

$$\int_{\Delta\Omega^l}\int_{\Delta A} I\,\vec{\Omega}.\vec{n}\,dA\,d\Omega=\int_{\Delta\Omega^l}\int_{\Delta v}\beta(R-I)\,dv\,d\Omega \quad (11)$$

ΔA are the surfaces of the control volume faces, one can write in algebraic form:

$$\sum_{i=1}^{6} I_i^l \Delta A_i\, N_i^l=\beta(R-I^l)\Delta v \quad (12)$$

with : $R=(1-\omega)I^0+\dfrac{\omega}{4\pi}\sum_{l'=1}^{L} I^{l'}\Delta\Omega^{l'}$ and $N_i^l=\dfrac{1}{\Delta\Omega^l}\int_{\Delta\Omega^l}\vec{\Omega}.\vec{n}_i\,d\Omega$ (13)

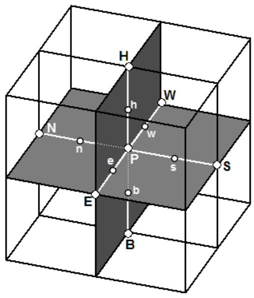

Fig. **2.** Volume control

Dimensionless radiant intensity at the diffuse borders is given by:

$$I_W^l=\frac{\varepsilon n^2\sigma T_W^4}{\pi}+\frac{(1-\varepsilon)}{\pi}\sum_{L_+}\left|N_w^{l'}\right|I_W^{l'}\Delta\Omega^{l'} \quad (14)$$

In the classical FVM, polar and azimuthal angles are uniformly subdivided in respectively N_θ and N_φ directions with a total of $N_\theta \times N_\varphi$ control angles (Fig. **3a**), in the FT*n*FVM [26], the polar angle is divided uniformly into a pair number *N*, whereas the azimuthal angle is divided uniformly into the following sequence of 4, 8, 12..., 2 *N*, 2*N* .., 12, 8, 4 in each level of the polar angle as shown in the fig. 3b. The total number of control solid angles is thus N(N +2). This new angular discretization of the finished volumes method was proposed by Kim and Huh [26] for three-dimensional radiative transfer of a semi-transparent medium which anisotropically absorbs, emits and diffuses the radiation.

Results obtained with the FT*n* FVM show a good agreement with reference solutions and are more precise than those obtained with the standard DOM or FVM for the same total number of controls angles. Indeed, FT*n* FVM produces a control solid angles distribution more uniform than the FVM.

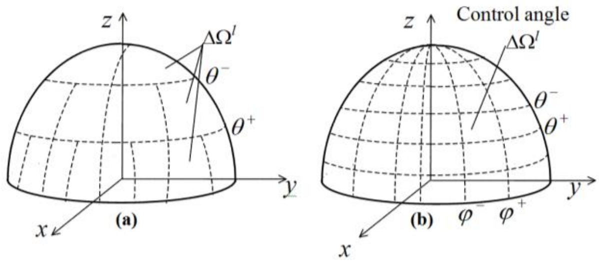

Fig. **3.** Angular Discretisation. a) FVM, b) FTnFVM

A times step equal to 10^{-4}, a space grid of 51^3 for Ar=1, 51x101x51 for Ar=2, 41x161x41 for Ar=4, and 31x241x31 for Ar=8 and an angular grid FT_6FVM were retained to extract simulations.

Conductive and radiative dimensionless fluxes are evaluated along the isothermal walls in the following way:

Local conductive flux:

$$q_c=-\frac{\partial T}{\partial x} \quad (15)$$

Local radiative flux:

$$q_r=\sum_{l=1}^{L}N^l I^l \Delta\Omega^l \quad (16)$$

The average values, on each wall, of these quantities are noted respectively $\overline{q_c}$ and $\overline{q_r}$.

3. Validation tests

The comparison of radiative and conductive fluxes on the heated wall, with the recent results of Colomer et al.[24], is presented, for several optical thicknesses, in table 1. A remarkable difference is observed between the two results but it is significant to announce that Colomer et al. [24] used the discrete ordinates method with suitable directions and for the classical 3D furnace case they compared their results only with the approximation P3 of the spherical harmonics.

4. Results and discussions

The effect of radiative transfer on principal flow characteristics and on the three-dimensional transverse flow is discussed for $Ra=10^5$, Pr=13.6, $\Phi_t = 0.1$, blacks isothermal walls and perfectly reflective adiabatic walls. The value of Prandtl number corresponds to $LiNbO_3$ in the liquid state which is a radiativly participating medium [25]**.** The effects of the conduction-radiation parameter, the optical thickness and the aspect ratio on the principal flow, the heat transfer and the transverse flow are discussed.

4.1 Effect of radiation on the principal flow and the heat transfer

In absence of any other indication, a gray semi-transparent medium not diffusing with $\tau = 1$ is considered. For Ar=2 and in absence of the radiative transfer, a ' chat eyes ' flow tilted towards the cold wall is established (fig. 4a). For larger aspect ratios (Ar=4 and Ar=8) flow becomes with only one vortex (fig. 4b and 4c), slightly tilted for Ar=2. Figure 4 shows also that for Ar=2 and Ar=4, the flow is with central symmetry but for Ar=8, the flow is with central and axial symmetries. When Rc increases, the flow in the center intensifies and only one vortex is observed (fig. 5, 6 and 7). For Ar=2 a grouping of two vortices is met, this grouping was already announced in two-dimensional simulation [24]. However, with a 3D model, streamlines in the XY plan are not closed.

For Rc=1 and Rc=10, the flow is with a vortex located in the center for all the values of Rc. For $Rc \rightarrow \infty$ the vortex, remains in the center for Rc=2, but it is localized in top of the cavity for higher values of Rc. Corresponding isothermal surfaces are represented on the fig. 8, 9 and 10, they highlight the significant reduction of the vertical stratification of the temperature in the center when the medium is radiatively participating. This dressing up of isotherms is due to the heating by radiation of the fluid near to the top of the hot wall and the bottom of the cold wall. One notes the three-dimensional distribution of the temperature for Rc=0.1 and 10. When $Rc \rightarrow \infty$, the temperature field becomes independent of the flow and a pure radiation profile is obtained. These isothermal surfaces are quasi-equidistant except near to the active walls.

By comparing figures 11 and 12, it is clear that the radiation increases the conductive transfer in the top of the hot wall and weakened it in the bottom and the reverse is true for the cold wall. Because of the temperatures levels difference, radiative flux is more significant on the hot wall (fig. 13) whereas conductive flux is more significant on the cold wall (fig. 12).

For Rc=0, they exist peaks of heat transfer in the top of the cold wall and the bottom of the hot wall (fig. 11). The radiation heat transfer tends to homogenize these distributions. For Rc=10 the homogenization is more significant for the weak aspect-ratios (fig. 13). When Rc→∞, the homogenization is more significant for the great aspect-ratios (fig. 14).

		τ = 0		τ = 1		τ =10	
		$\overline{q}_c$	$\overline{q}_r$ Rc/Φ_t	$\overline{q}_c$	$\overline{q}_r$ Rc/Φ_t	$\overline{q}_c$	$\overline{q}_r$ **Rc/Φ_t**
Ra = 10^3	Our results	1.06	6.49	1.70	4.61	1.65	**1.25**
	Colomer et al. [24]	1.76	6.20	1.76	4.64	1.54	**1.16**
Ra = 10^4	Our results	2.04	6.89	2.45	5.12	2.23	**1.65**
	Colomer et al. [24]	2.26	6.28	2.25	4.69	2.11	**1.54**
Ra = 10^5	Our results	4.13	7.23	4.04	5.88	4.46	**2.99**
	Colomer et al. [24]	**4.37**	**6.52**	**3.92**	**5.44**	**4.21**	**2.8**

Table 1. Comparison of thermal transfer on the hot face between our results and those of the literature for Pr=0.71, Rc=1/(0.016×17) et Φ_t=1/17.

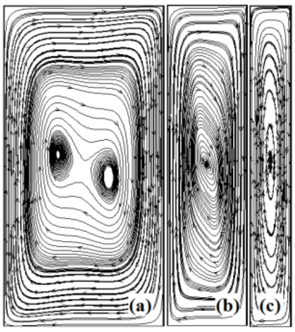

Fig. 4. Projection of the velocity vectors on the median plane (XY) for Ra=10^5, Pr=13.6 and Rc = 0 (without radiation), (a): Ar=2, (b): Ar=4, (c): Ar=8

These influences of the radiative transfer on the natural convection are similar to those obtained for the air with 3D[24] and 2D [23] modeling. As waited, when Rc→∞, the radiative fluxes distributions do not express any effect of gravity and are practically identical on the heated and cooled walls (fig. 14). Moreover, Colomer et al. [24] observed an increase in these fluxes at both ends of z axis this variation is more significant for optical thin media.

Figures 11 and 12 show also that the effects of the vertical adiabatic walls on the conductive transfer are more pronounced at the bottom of the hot face and the top of the cold face. The reverse is true for radiative flux (fig. 13 and 14).

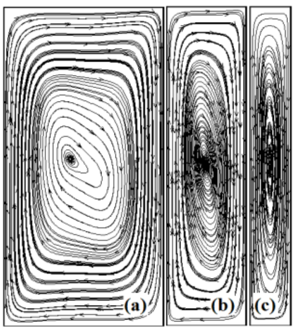

Fig. 5. Projection of the velocity vectors on the median plane (XY) for Ra=10^5, Pr=13.6 and Rc =1, (a) : Ar=2, (b) : Ar=4, (c) : Ar=8

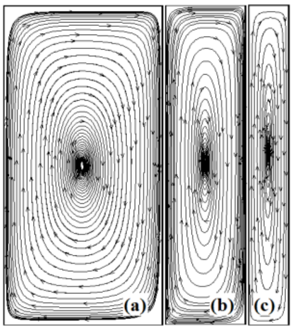

Fig. 6. Projection of the velocity vectors on the median plane (XY) for Ra=10^5, Pr=13.6 and Rc =10, (a) : Ar=2, (b) : Ar=4, (c) : Ar=8

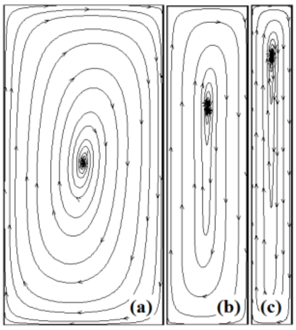

Fig. 7. Projection of the velocity vectors on the median plane (XY) for Ra=10^5, Pr=13.6 and Rc Rc →∞, (a) : Ar=2, (b) : Ar=4, (c) : Ar=8

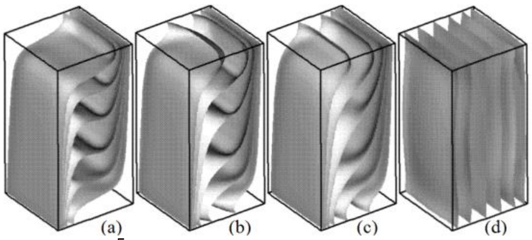

Fig. 8. Isothermal surfaces for : Ra=10^5, Pr=13.6, $\Phi_t = 0{,}1$ and Ar=2 ; a) Rc = 0 (without radiation), b) Rc =1, c) Rc = 10 et d) Rc = ∞.

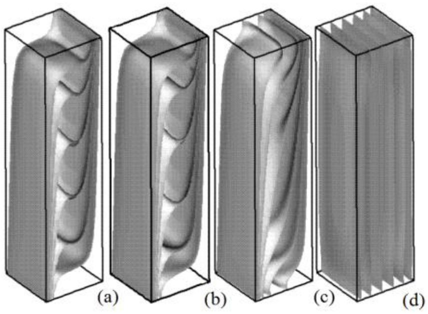

Fig. 9. Isothermal surfaces for : Ra=10^5, Pr=13.6, $\Phi_t = 0{,}1$ and Ar=4 ; a) Rc = 0 (without radiation), b) Rc =1, c) Rc = 10 et d) Rc = ∞.

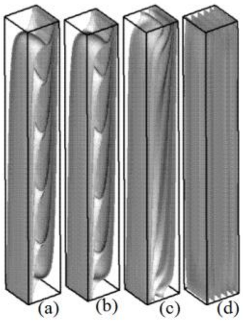

Fig. 10. Isothermal surfaces for : Ra=10^5, Pr=13.6, $\Phi_t = 0{,}1$ and Ar=8 ; a) Rc = 0 (without radiation), b) Rc =1, c) Rc = 10 et d) Rc = ∞.

The results concerning the effects of the optical properties on the heat transfer on the active walls are qualitatively identical to the square cavity case [23], the optical thickness has a more significant influence that the scattering albedo. Table 2 summarize the effect of the optical thickness on the heat transfer through the active walls for Rc=10 and various values of aspect-ratio. The results for τ =0.01 and 100 are very close to those for respectively τ =0.1 and 10. The great dependence between $\overline{q}_r$ and τ is also found in this table. For a fixed optical thickness the increase in the aspect ratio generates a reduction in the average conductive flux on the isothermal walls. Radiative flux is maximum for Ar=4.

4.2 Effect of radiation on the transverse flow

In this part we present results concerning the influence of the radiative transfer on the transverse three-dimensional flow for Pr = 13.6 and Ra = 10^5.

The transverse flow is a direct demonstration of 3D nature of the movement and it is of primary importance to study instationnarity and transitions. This three-dimensional movement is generated by the presence of the adherent walls to the fluid [1] which cause a 3D effect known as inertia-effect and by another 3D effect says thermal-effect due to temperature variation in close to the side walls.

In the air Rayleigh-Benard convection case, Kessler [18] mentioned that these heating effects are restricted at a small zone close to the walls whereas the effects of inertia are perceptible in all the enclosure. Indeed, and like already indicated, the fluid particles which move in the xy plans do not remain in the same plan and a weak ' hélicoïdal' flow exists. The velocity component corresponding (V_z) is in general smaller of an order of magnitude than the components of the principal flow (V_x and V_y) [15]. Contrary to the two-dimensional situation, projection of the velocity vectors on the median plane XY are not closed but describe spirals in direction of the centers of the vortices or in direction of the walls.

For Ar=2 and in absence of radiation (fig. 15), a complexes transverse flow occurs. Two central movements in spirals exist and converge towards an intermediate xy plan located at z ≈ 0.85 (fig. 15a-b). This is followed by a divergent flow to the front wall as shown in these figures. We noted thereafter the appearance of a succession of flows in convergent, divergent spirals then again convergent, between this wall and plan XY (fig. 15c-d).

For Ar=4 (fig. 16) the flow becomes with only one vortex and the external flow becomes more organized with a more reduced passage of a plan towards another.

As mentioned above, projection of the velocity vectors in the xy plans are not closed. This is confirmed in the fig. 17a which shows the convergent movement towards the two vortices in xy plans. This structure is modified for z = 0.9 and the peripheral flow develop in spirals towards the walls (fig. 17b). This structure persists until z=0.99 (fig. 17c) and consequently no merging of vortices is observed. While in the center, the flow remains convergent towards the centers of these vortices. For Ar=4 (fig. 18) and Ar=8, the flow is with only one vortex for all the xy plans.

For Ar=2 (fig. 19), the results above are clearly changed. For Rc = 1 and τ = 0.1, the flow becomes with only one slightly tilted vortex towards the hot wall, developing in convergent- inners and divergent-peripherals spirals.

The peripheral converge flow is similar to that obtained in pure natural convection. By increasing Rc (fig. 20) the vortex is not inclined any more and the flow becomes more and more organized. For Ar=4 and 8, Rc = 1 and τ = 0.1, the flow always remains with only one vortex with a structure almost identical to that in absence of the radiation.

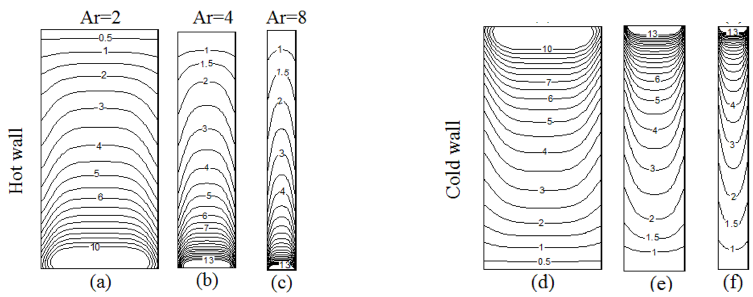

Fig. 11. Conductive fluxes distribution on the isothermal walls for Rc=0, Ra=10^5, Pr=13.6 and $\Phi_t = 0{,}1$

For aspect ratio higher than 2, and when Rc tends towards the infinite, one notices that the center of the vortex changes position into passing from a plan towards another. For example for Ar=4 (fig. 21), for z=0.5 the vortex is localized in the top of the cavity, for z=0.75 it is localized perfectly at the center of the cavity and for z=0.85 it becomes in bottom of the cavity.

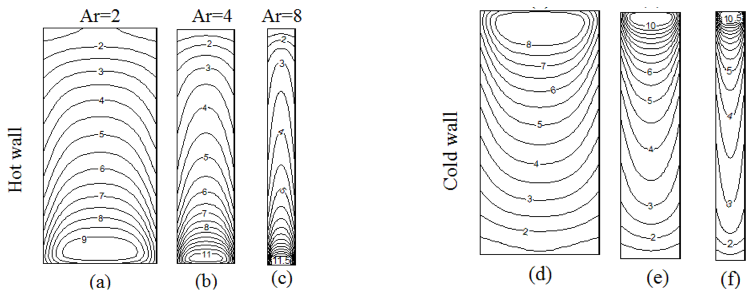

Fig. 12. Conductive fluxes distribution on the isothermal walls for Rc=10, Ra=10^5, Pr=13.6 and $\Phi_t = 0{,}1$

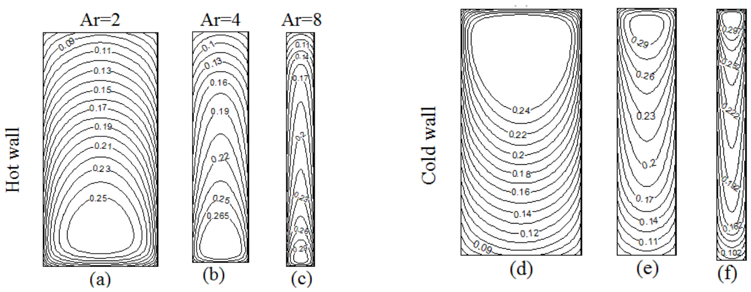

Fig. 13. Radiative fluxes distribution on the isothermal walls for Rc=10, Ra=10^5, Pr=13.6 and $\Phi_t = 0{,}1$

Figure 22, shows the variations of the transverse velocity maximum V_{zmax} according to the aspect ratio for various values of Rc. Transverse velocity increases according to Rc and Ar, which implies that the increase in Rc and Ar, increases the three-dimensional aspect of the flow.

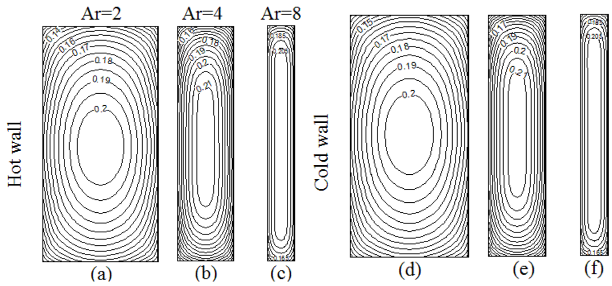

Fig. 14. Radiative fluxes distribution on the isothermal walls for Rc $\rightarrow \infty$, Ra=10^5, Pr=13.6 and $\Phi_t = 0{,}1$

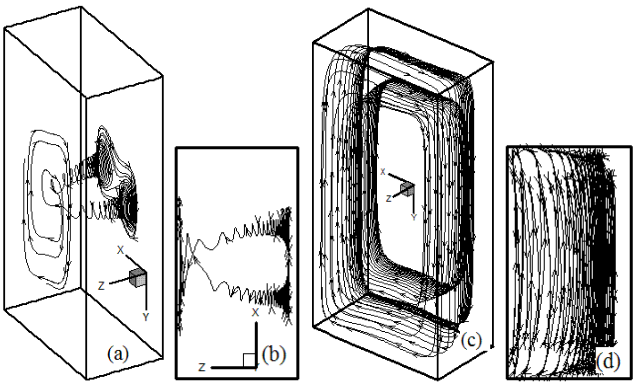

Fig. 15. Some particle tracks in absence of radiation, for Pr = 13.6, Ar=2, Rc=0 and Ra=10^5 showing inner spiraling flows ((a) and (b)) and 'peripheral' spiraling flows ((c) and (d)).

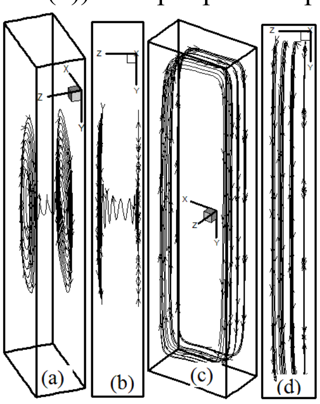

Fig. 16. Some particle tracks in absence of radiation, for Pr = 13.6, Ar=4, Rc=0 and Ra=10^5 showing inner spiraling flows ((a) and (b)) and 'peripheral' spiraling flows ((c) and (d)).

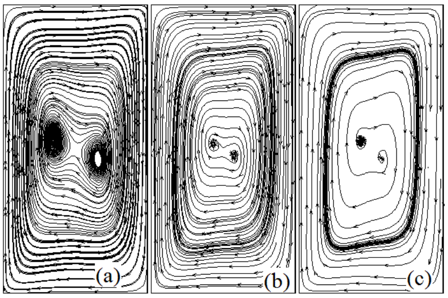

Fig. 17. Projection of the velocity vectors in absence of the radiation for Ar=2, Pr = 13.6 et Ra=10^5.a) z=0,6 b)z=0,9 c) z=0.99

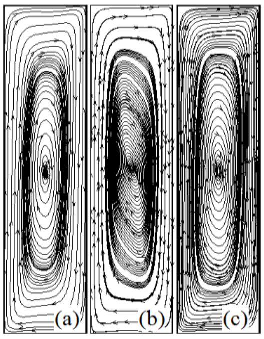

Fig. 18. Projection of the velocity vectors in absence of the radiation for Ar=4, Pr = 13.6 et Ra=10^5.a) z=0,6 b)z=0,9 c) z=0.99

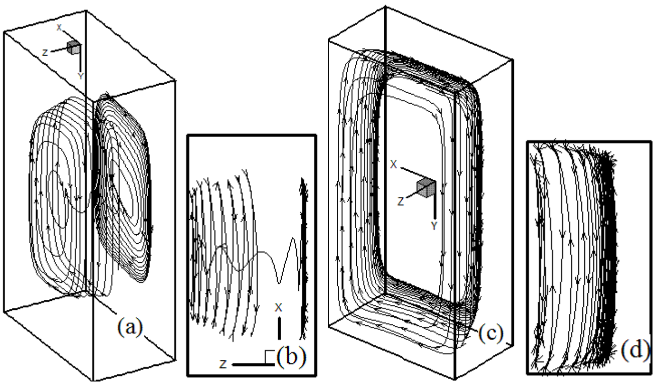

Fig. 19. Some particle tracks, for Rc=1, Pr = 13.6, Ar=4, Rc=0 and Ra=10^5 showing inner spiraling flows ((a) and (b)) and 'peripheral' spiraling flows ((c) and (d)).

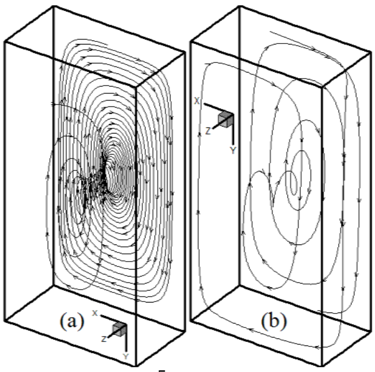

Fig. 20. Particle tracks for Ar=2, Ra=10^5, Pr=13.6 et $\Phi_t = 0{,}1$; (a) Rc=10, (b) Rc$\rightarrow\infty$

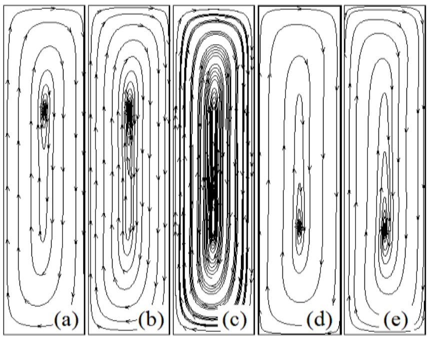

Fig. 21. Projection of the velocity vectors in for Rc→∞, Ar=4, Pr = 13.6 et Ra=10^5. a) z=0,5 b)z=0,65 c) z=0.75 d)z=0,85 e) z=0.95

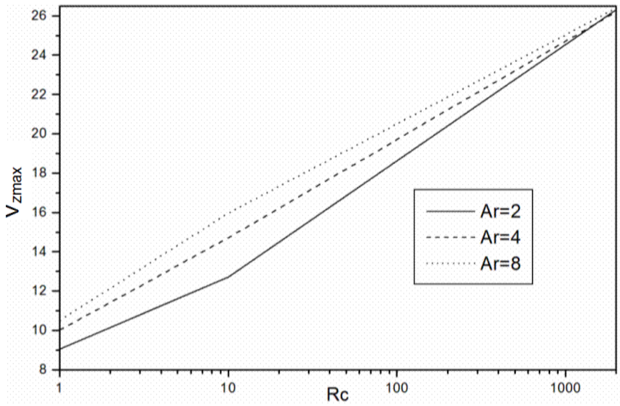

Fig. 22. Influence of Rc and Ar on maximum transverse velocity. For Ra=10^5, Pr=13.6, τ= 1 and $\Phi_t = 0{,}1$.

Rc=10		Hot wall		Cold wall	
τ	Ar	$\bar{q}_c$	$\bar{q}_r\, Rc/\Phi_t$	$\bar{q}_c$	$\bar{q}_r\, Rc/\Phi_t$
0.1	2	4.376	25.003	4.535	23.570
	4	4.091	27.130	4.241	25.839
	8	3.485	27.868	3.630	26.645
1	2	4.568	18.949	5.014	18.021
	4	4.421	19.770	4.862	18.917
	8	3.984	19.559	4.378	18.745
10	2	5.121	9.098	5.734	8.453
	4	4.545	9.469	5.175	8.839
	8	3.927	8.313	4.476	7.754

Table 2. Effect of optical thickness and aspect ratio on the heat transfer for Rc=10, Ra = 10^5, Pr = 13.6 and $\Phi_t = 0{,}1$.

5. CONCLUSION

The results presented in this article relate to lengthened three-dimensional enclosures differentially heated, these results are carried out for Pr=13.6.

In absence of radiation there is a zone not far from the median plane where the flow is quasi-two-dimensional. The transverse flow developing in interior spirals starts halfway between this plan and the front and back walls.

The effect of the radiation heat transfer on the 3D behavior of the flow is significant in the heart of enclosure. The flows developing in interior spirals are very sensitive in position and direction to the radiation, while the movement developing in peripheral spirals is qualitatively not very sensitive to this mode of transfer. This postulates that the radiative transfer transports the 3D heating effect to the major part of the cavity.

For the weak aspect ratios, in the absence of the radiation the flow is two vortices and no combination of the two vortices is announced. However, for a semi-transparent medium the flow is with only one vortex.

When the radiation conduction parameter tends towards infinite the position of the vortex passes from the top of the cavity downwards and passing from a transversal plan towards another.

Nomenclature

Ar	– aspect ratio
$\vec{g}$	– acceleration of gravity
H	– height of the cavity
i	– refractive index
I	– dimensionless radiant intensity, $\left(= I\ '/(i^2\sigma(T_c')^2/\pi)\right)$
I^0	– dimensionless black body intensity, $\left(= I^0{}'/(i^2\sigma(T_c')^2/\pi)\right)$
L	– total number of discrete solid angles
n	– unit vector normal to the control volume surface
P	– pressure
Pr	– Prandtl number $(= \nu/\alpha)$
q_c	– dimensionless local conductive heat flux on isothermal walls
q_r	– dimensionless local radiative heat flux on isothermal walls
Ra	– Rayleigh number
Rc	– radiation conduction parameter $(= i^2.W.T'^3_c.\sigma/\lambda)$
s	– distance in the direction Ω of the intensity
t	– dimensionless time,
T	– dimensionless temperature
T_c	– colde temperature
T_h	– hot temperature
$\vec{V}$	– velocity vector
W	– cavity width

Greek symbols

α	– thermal diffusivity
β	– extinction coefficient
β_t	– coefficient of thermal expansion
ΔA	– area of a control volume face
ΔV	– control volume
$\Delta\Omega^l$	– control solid angle
ε	– emissivity
Φ_t	– temperature ratio

κ	– absorption coefficient
$\vec{\psi}$	– dimensionless vector potential
ν	– kinematic viscosity
σ	– Stefan–Boltzmann constant
τ	– optical width
$\vec{\omega}$	– dimensionless vorticity vector
ω_0	– scattering albedo
$\vec{\Omega}$	– unit vector in the direction of the intensity

Subscript

x, y, z	– Cartesian co-ordinates

Superscript

'	– real variables
l, l'	– discrete angular directions

References

[1] Mallinson, G. D., De Vahl Davis, G., Three-dimensional natural convection in a box: a numerical study. *J. Fluid Mech. 83* (1977), pp. 1-31.

[2] Lee, T. S., Son, G. H., Lee, J. S. Numerical predictions of three dimensional natural convection in a box. Proc. *1st KSME-JSME Thermal and Fluid Engineering Conference. 2,* (1988), pp. 278-283.

[3] Hiller, W. J., Koch, S., Kowaleweski, T. A.,. Three-dimensional structures in laminar natural convection in a cubic enclosure. *Exp. Thermal. And Fluid Science. 2*, (1989), pp. 34-44.

[4] Hiller, W. J., Koch, S., Kowaleweski, T. A., de Vahl Davis, G., Behnia, M., Experimental and numerical investigation of natural convection in a cube with two heated side walls. Proc. *Int. Union of Theoretical and Applied Mechanics Symposium.* (1990), pp. 717-726.

[5] Fusegi, T., Hyun, J. M., Kuwahara, K., Farouk, B., A numerical study of three-dimensional natural convection in a differentially heated cubical enclosure. *Int. J. Heat Mass Transfer. 34*, (1991), pp. 1543-1557.

[6] Fusegi, T., Hyun, J. M., Kuwahara, K., A numerical study of 3-D natural convection in a cube: effects of the horizontal thermal boundary conditions. *Fluid Dynamics Research. 8,* (1991), pp. 221-230.

[7] Janssen, R. J. A., Henkes, R. A W. M, Hoogendoorn, C. J.,. Transition to time-periodicity of a natural-convection flow in a 3D differentially heated cavity. *Int. J. Heat Mass Transfer. 36*, (1993), pp. 2927-2940.

[8] Kowalewski, T. A., Experimental validation of numerical codes in thermally driven flows. *Adv. in Computational Heat Transfer*, (1998), pp. 1-15.

[9] Leonardi, E., Kowalewski, T. A., Timchenko, V., De Vahl Davis, G., Effects of finite wall conductivity on flow structures in natural convection. *CHMT Cyprus April* (1999), pp., 182-188.

[10] Tric, E., Labrosse, G., Betrouni, M., A first incursion into the 3D structure of natural convection of air in a differentially heated cubic cavity, from accurate numerical solutions. *Int. J. Heat Mass Transfer. 43*, (2000), pp. 4043-4056.

[11] Pepper, D. W., Hollands, K. G. T.,. Summary of benchmark numerical studies for 3-D natural convection in an air-filled enclosure. *Numerical Heat Transfer, Part A. 42*, (2002), 1-11.

[12] Wakashima, S., Saitoh, T. S., Benchmark solutions for natural convection in a cubic cavity using the high-order time-space method. *Int. J. Heat Mass Transfer. 47*, (2004), pp. 853-864.

[13] Le Peutrec, Y., Lauriat, G.,. Effects of the heat transfer at the side walls on natural convection in cavities. *J. Heat Transfer. 112*, (1990), pp. 370-378.

[14] Viskanta, R., Kim, D. M., Gau, C., Three-dimensional natural convection heat transfer of a liquid metal in a cavity. *Int. J. Heat Mass Transfer. 29*, (1986), pp. 475-485.

[15] Henry, D., Buffat, M., Two and three-dimensional numerical simulations of the transition to oscillatory convection in low-Prandtl fluids. *J. of Fluid Mechanics. 374*, (1998), pp. 145-171.

[16] Juel, A., Mulin, T., Ben Hadid, H., Henry, D., Three-dimensional free convection in molten gallium. *J. of Fluid Mechanics. 436*, (2001), pp. 267-281.

[17] Piazza, I. D., Ciofalo, M.,. MHD free convection in a liquid-metal filled cubic enclosure. I. Differential heating. *Int. J. Heat Mass Transfer. 45*, (2002), pp. 1477-1492.

[18] Kessler, R.,. Nonlinear Transition in Three-Dimensional Convection. *J. of Fluid Mechanics. 174*, (1987), pp. 357-379.

[19] Chang, L.C., Yang, K. T., Lioyd, J. R.,. Radiation-natural convection interactions in two-dimensional complex enclosures. *J. Heat Transfer.105*, (1983), pp. 89-95.

[20] Yang, K. T., Numerical modelling of natural convection-radiation interactions in enclosures. In Heat Transfer 1986: Proc. *Eighth Int. heat Transfer Conf. 1*, (1986), pp. 131-140.

[21] Yucel, A., Acharaya, S., Williams, M. L., Natural convection and radiation in a square enclosure. *Numerical. Heat Transfer. 15*, (1989), pp. 261-277.

[22] Fusegi, T., Farouk, B., Laminar and turbulent natural convection-radiation interactions in a square enclosure filled with a nongray gas. *Numerical Heat Transfer. 15*, (1989), pp. 303-322.

[23] Tan, Z., Howell, J. R., Combined radiation and natural convection and in a two-dimensional participating square medium. *Int. J. Heat Mass Transfer. 34*, (1991), pp. 785-793.

[24] Colomer, G., Costa, M., Cònsul, R., Oliva, A., Three-dimensional numerical simulation of convection and radiation in a differentially heated cavity using the discrete ordinates method. *Int. J. Heat Mass Transfer. 47*, (2004), pp. 257-269.

[25] Kobayachi, M., Tsukada, T., Hozawa, M., Effect of internal radiative heat transfer on transition of flow modes in CZ oxide melt, *J. Crystal Growth. 208*, (2000), pp. 459-465.

[26] Kim S.H., Huh K. Y. A new angular discretization scheme of the finite volume method for 3-D radiative heat transfer in absorbing, emitting and anisotropically scattering media. *Int J Heat Mass Transfer. 43*, (2000), pp. 1233-1242.

[27] Chai J.C., Lee H.S., and Patankar S.V., Finite Volume Method for Radiation Heat Transfer, *Journal of Thermophysics and Heat Transfer. 8*, (1994), pp. 419-425.

Affiliation

Ecole Nationale d'Ingénieur de Monastir, Monastir, Tunisia. E-mail : lioua_enim@yahoo.fr